

双光束激光填丝焊工艺对铝合金焊接气孔率的影响

雷正龙¹, 李 颖¹, 陈彦宾¹, 孙忠绍², 张益坤²

(1. 哈尔滨工业大学 先进焊接与连接国家重点实验室, 哈尔滨 150001; 2. 首都航天机械公司, 北京 100076)

摘 要: 以 LF6 铝合金为材料, CO₂ 激光为热源, 开展了双光束激光填丝焊气孔特性分析。与单光束激光填丝焊及双光束自熔焊相比, 双光束激光填丝焊能够抑制气孔的产生, 尤其是并行双光束激光焊抑制气孔效果更明显。在此基础上进一步分析了保护气体成分和激光能量对焊接气孔率的影响。结果表明, 采用氦气保护时, 等离子体对激光的屏蔽作用小, 能够稳定焊接过程; 激光功率过大或者过小都会导致匙孔的不稳定, 造成焊缝气孔率增加。

关键词: 双光束激光填丝; 气孔; 工艺参数; 铝合金

中图分类号: TG456.7 文献标识码: A 文章编号: 0253-360X(2013)02-0040-05



雷正龙

0 序 言

激光焊具有能量密度高、热影响区及焊接热变形小、焊缝深宽比大(可达 12:1)、自动化程度高和不需要真空保护等特点, 使得激光焊具有广泛地应用前景, 被认为是 21 世纪最先进的焊接方法之一^[1]。但铝合金对激光具有极高的反射和导热性, 特别是对于波长为 10.6 μm 的 CO₂ 激光反射率高达 97% 以上。同时 Al 元素的电离能低, 焊接过程中光致等离子体易于过热和扩展, 导致焊接匙孔不稳定, 易产生气孔; 此外铝合金中低熔点成分在高功率密度的激光能量辐照下极易蒸发, 增大了气孔的产生的倾向^[2,3]。

针对铝合金激光焊气孔的形成机制, 目前大多数学者认为是由于焊接过程中匙孔前壁的不稳定导致的^[4]。同时铝合金凝固过程中氢的聚集也会导致气孔的产生^[5]。针对铝合金气孔的抑制, 有学者提出了双光束激光焊的方法。相比单光束激光焊, 双光束激光焊匙孔宽且浅, 匙孔不易塌陷, 并且焊接过程中匙孔始终处于张开状态, 抑制了等离子体的喷发, 从而使焊接过程更加稳定, 气孔产生倾向减小, 但是气孔仍然是铝合金焊缝的主要缺陷^[6,7]。

文中将以航天领域常用的 LF6 铝合金为对象, 以 CO₂ 激光为热源, 通过分光系统将单束激光分为双束激光, 进行了铝合金双光束激光填丝焊接试验,

分析了不同工艺参数对气孔率的影响规律。

1 试验方法

试验所选用的母材为防锈铝合金 LF6(国际牌号为 5A06), 尺寸为 300 mm × 50 mm, 厚度为 2 mm。采用的焊丝型号为 ER5356, 直径为 1.2 mm。母材与焊丝成分见表 1 和表 2。

表 1 5A06 铝合金化学成分(质量分数, %)

Table 1 Chemical compositions of 5A06 aluminum alloy

Mg	Mn	Fe	Si	Ti	Be	Al
6.8	0.5~0.8	≤0.4	≤0.4	0.02~0.01	0.001~0.005	余量

表 2 ER5356 铝合金焊丝化学成分(质量分数, %)

Table 2 Chemical compositions of ER5356 aluminum wire

Mg	Mn	Cu	Zn	Si	Cr	Ti	Al
5.0	0.1	—	—	—	0.1	0.1	余量

激光器采用德国 Rofin 公司的 DC030 型 CO₂ 激光器。双光束采用并行和串行排布两种模式, 双光束激光光束间距为 0.6 mm。焊接过程中采用前送丝、后吹保护气体模式, 如图 1 所示, 将送丝喷嘴及保护气喷嘴以一定角度固定在激光头上, 焊接时保持静止, 工件移动。同时送丝喷嘴夹具应具有一定的刚度, 以保证送丝过程稳定。在试验中如无特殊说明, 均采用并行排布方式试验。

为研究焊接过程稳定性对于焊缝气孔的影响,

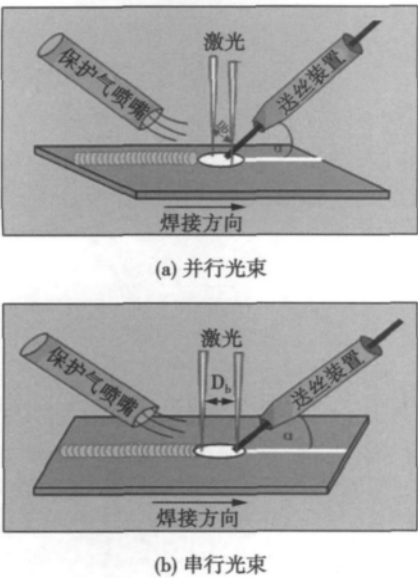


图 1 双光束焊接示意图
Fig. 1 Schematic diagrams of dual-beam laser welding

采用 CCD 拍摄激光焊过程中产生的等离子体 ,根据等离子体的波动情况 ,判断焊接过程的稳定性. 利用 MATLAB 软件编写相关程序 ,对拍摄的等离子体进行二值化处理 ,得到等离子体轮廓图 ,然后计算等

离子体相对面积 ,得到等离子体大小随时间变化的曲线 ,从而判定焊接过程的稳定性.

2 焊接工艺参数对气孔率的影响

气孔率的计算参考欧洲 ISO13919—2: 2001 铝合金激光焊质量等级标准进行计算 ,为了可靠地比较不同焊接方法下气孔率的大小 ,对相同条件下 5 次试验结果取平均值进行了比较分析(以下同) .

2.1 填充焊丝的影响

焊丝的加入可以改变熔池的温度场以及焊接过程的稳定性 ,同时也可以改善焊缝成形(表 3) ,双光束激光自熔焊时 ,焊缝下塌 ,容易形成应力集中 ,焊缝力学性能降低 ,而填丝焊接时 ,焊缝成形良好 ,正反面均有一定的余高 ,改善了应力集中状态. 不填丝焊缝气孔率为 5. 39% ,填丝焊缝气孔率为 3. 71% ,焊丝的加入减小了气孔倾向.

2.2 光束排布形式的影响

不同的光束形式 ,会形成不同的焊接匙孔 ,造成焊接过程稳定性的差异 ,从而导致气孔倾向的不同. 表 4 显示了不同光束排布形式的双光束激光与单激光填丝焊接的焊缝成形及其 X 光照片 ,可以看出 ,

表 3 填加焊丝影响
Table 3 Influence of wire on porosity rate

激光功率 P/W	焊接速度 $v_w/(m \cdot min^{-1})$	送丝速度 $v_s/(m \cdot min^{-1})$	焊缝成形	X 射线底片
1 800	1. 5	0		
1 800	1. 5	1. 8		

表 4 光束形式比较
Table 4 Comparison of different arrangement of dual - beam

工艺参数	光束形式	焊缝成形	X 射线底片
$P=2\ 200\ W$ $v_w=2.0\ m/min$ $v_s=2.5\ m/min$	单光束		
$P=2\ 200\ W$ $v_w=2.0\ m/min$ $v_s=2.5\ m/min$	串行双光束		
$P=2\ 200\ W$ $v_w=2.0\ m/min$ $v_s=2.5\ m/min$	并行双光束		

与单激光焊相比,双光束激光焊不仅可以改善焊缝成形,而且可以显著减少气孔产生.

图 2 显示了不同光束形式作用下气孔率的大小.单光束激光填丝焊气孔率最高,达到 4.6% 以上,串行双光束其次,并行双光束焊接气孔率最低,为 2.5% 左右.这主要是因为采用双光束进行焊接时,两束光形成一个相对较大的匙孔,提高了匙孔的稳定性,有利于气体的逸出.此外采用并行双光束焊接时,熔池内部温度梯度更小,降低了液态金属凝固速度,延长了气泡的逸出时间,有利于减小气孔倾向;同时并行双光束激光焊也有利于提高送丝的稳定性的,因此在铝合金双光束激光填丝焊过程中,主要采用并行双光束进行焊接.

2.3 保护气体成分的影响

由于铝合金激光焊接过程会产生较大的等离子体,等离子体对激光具有一定的屏蔽作用,且易导致匙孔不稳定而产生气孔.因此焊接过程中除采用保护气体对焊接区进行保护之外,还须利用保护气抑

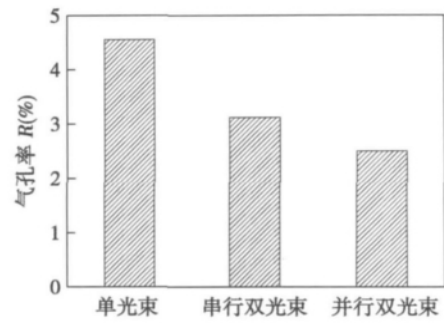


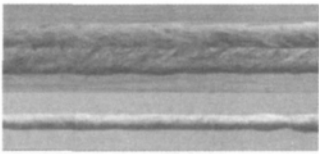
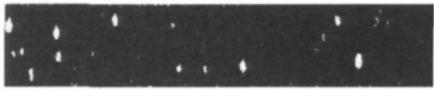
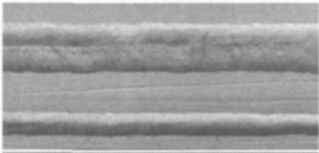
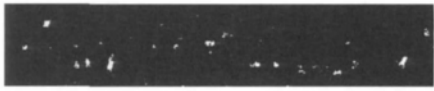
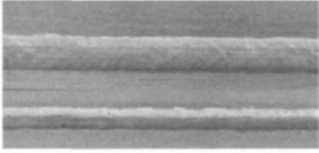

图 2 不同光束形式作用下的气孔率

Fig. 2 Porosity rate under action of different arrangement of dual-beam

制部分等离子体.表 5 显示了不同保护气成分下铝合金双光束激光填丝焊接的焊缝成形和 X 光气孔照片.随着保护气体中氦气含量的增加,不仅改善焊缝成形,表面熔宽减小,熔深增加,而且焊接气孔率明显降低,当完全采用氦气保护进行焊接时,焊缝气孔率最小,可以控制在 1% 以下,如图 3 所示.

表 5 保护气体成分的影响

Table 5 The influence of shielding gas on porosity rate

工艺参数	保护气体成分	焊缝成形	X 射线底片
$P=2\ 200\ \text{W}$ $v=2.0\ \text{m/min}$ $v_w=2.5\ \text{m/min}$	100% Ar		
$P=2\ 200\ \text{W}$ $v=2.0\ \text{m/min}$ $v_w=2.5\ \text{m/min}$	70% Ar + 30% He		
$P=2\ 200\ \text{W}$ $v=2.0\ \text{m/min}$ $v_w=2.5\ \text{m/min}$	100% He		

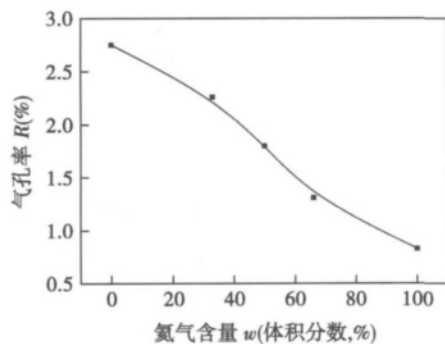


图 3 气孔率变化曲线

Fig. 3 Variation of porosity rate

通过 CCD 拍摄不同保护气体成分下等离子体形态可以发现,采用纯氦气保护时,工件表面形成的等离子体体积明显减小,并且波动范围相比纯氩气保护也大幅减小,焊接过程更加稳定,如图 4 所示.激光焊过程中,等离子体主要是由金属等离子体与保护气电离形成的等离子体组成.氦的电离能高(24.46 eV)难电离,使用纯氦气保护时,等离子体主要由金属等离子体组成;氩的电离能相对较低(15.69 eV),使用纯氩气保护时,等离子体由金属等离子体与氩等离子体共同组成.此外,氦气的导热性能要远优于氩的导热性能,使用氦气保护能够

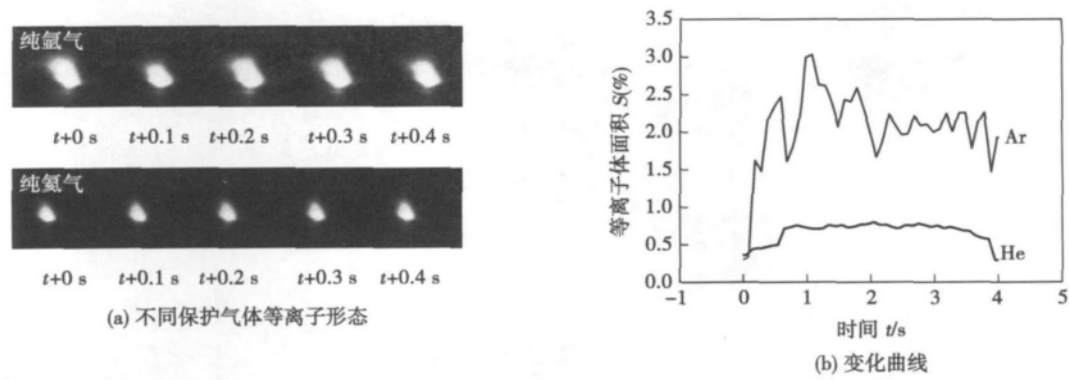


图 4 不同保护气体作用下等离子体波动情况
Fig. 4 Plasma fluctuations under action of different shielding gas

使等离子体的热量较快地散失,降低了等离子体的温度,从而抑制了等离子体长大的趋势. 因此使用氦气保护时,等离子体对激光能量的屏蔽作用减小,焊接过程更加稳定,降低气孔产生倾向.

2.4 激光功率的影响

激光功率的大小,影响熔池的温度梯度、冷却速

率和焊接过程稳定性,从而导致铝合金激光焊气孔率不同. 表 6 显示了采用氦气保护时不同功率下双光束激光焊时的焊缝成形及其 X 光照片. 可以发现,激光功率过大或过小,即焊缝过透或未透都会增大气孔倾向,当双光束激光功率为 2 200 W 左右时,焊缝气孔率达到最小,如图 5 所示.

表 6 激光功率的影响
Table 6 Influence of laser power

焊接速度 $v_w/(\text{m}\cdot\text{min}^{-1})$	激光功率 P/W	送丝速度 $v_s/(\text{m}\cdot\text{min}^{-1})$	焊缝成形	X 射线底片
2.0	2 600	3.4		
2.0	2 200	2.5		
2.0	1 800	2.0		

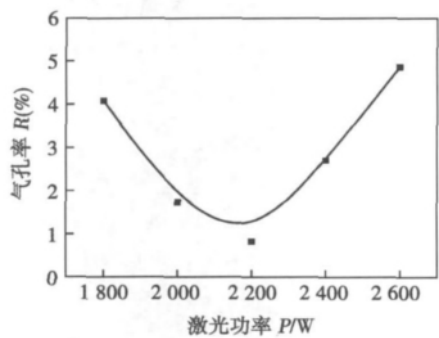


图 5 气孔率变化曲线
Fig. 5 Variation of porosity rate

图 6 显示了不同激光功率下双光束激光填丝焊的等离子体形态及其波动幅度变化规律. 从图 6 可以看出,图 6a 和图 6c 显示的激光等离子体体积大小随时间变化都发生了明显的波动,而图 6b 显示的激光等离子体演变过程中等离子体体积大小基本一致,这与图 6d 显示的结果是一致的. 由于激光焊接等离子体形态波动可以反映焊接过程的稳定性,当功率过大或者过小都会加剧等离子体的波动幅度,影响达到工件表面的激光能量,使焊接过程变得不稳定,从而影响焊接气孔的产生,这也是激光功率变化影响气孔率的主要原因.

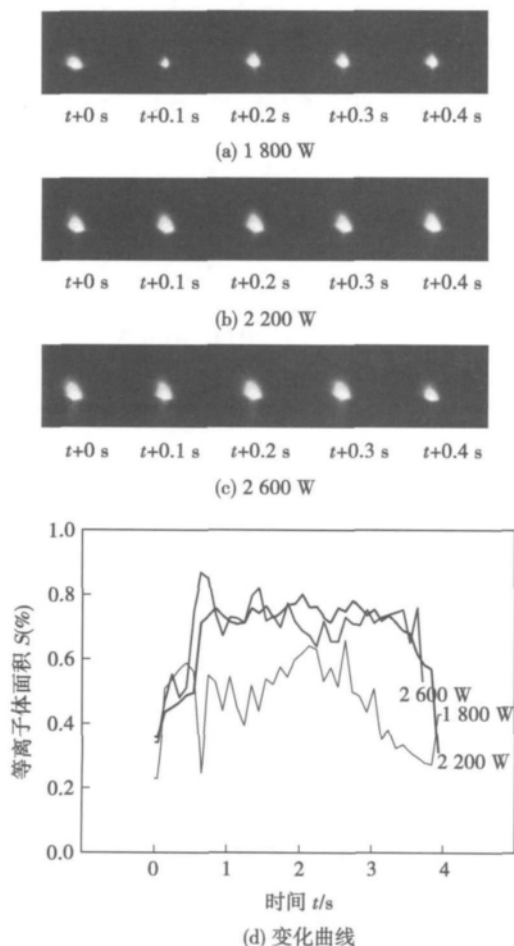


图 6 不同激光功率作用下等离子体波动情况

Fig. 6 Plasma fluctuations under action of different laser power

3 结 论

(1) 与单激光填丝焊及双光束自熔焊相比,双光束激光填丝焊可以在一定程度上抑制气孔的产生,且并行双光束的抑制能力要强于串行双光束。

(2) 氦气保护对铝合金激光焊接气孔的抑制作用比氩气保护明显。采用纯氦气保护时,匙孔波动

减弱,焊接区内等离子体减小,焊接过程更稳定,能够得到具有较好成形和稳定质量的焊缝,气孔率达到 1% 以下。

(3) 铝合金双光束激光填丝焊接过程中,功率过小或者过大都会使焊接过程不稳定而增大气孔倾向,在氦气保护和焊接速度为 2 m/min 的前提下,激光功率在 2 200 W 左右时,气孔率达到最小。

参考文献:

- [1] 左铁钊. 高强铝合金的激光加工[M]. 北京: 国防工业出版社, 2002.
- [2] 张赵林, 程兆谷, 雒江涛. 激光焊接铝合金的研究[J]. 中国激光, 1998, 25(5): 477-480.
Zhang Zhaolin, Cheng Zhaogu, Luo Jiangtao. Study of laser welding of aluminum alloys[J]. Chinese Journal of Laser, 1998, 25(5): 477-480.
- [3] 王希靖, 片山圣二. 不同铝合金在激光焊接时的熔化和蒸发特性[J]. 焊接学报, 1995, 16(1): 30-35.
Wang Xijing, Seiji K. Character of melting and evaporation in laser welding for different aluminum alloys[J]. Transactions of the China Welding Institution, 1995, 16(1): 30-35.
- [4] Matsunawa A, Mizutani M, Katayama S. Porosity formation mechanism and its prevention in laser welding[J]. Welding International, 2003, 17(6): 431-437.
- [5] Pastor M, Zhao H, Martukanitz R P. Porosity underfill and magnesium lose during continuous wave Nd: YAG laser welding of thin plates of aluminum alloys 5182 and 5754[J]. Welding Journal, 1999, 78(6): 207-216.
- [6] Kimihiro S, Takakuni I, Hiroki S. Process stabilization by dual focus laser welding of aluminum alloys for car body[C]// International Conference on Laser, Applications and Technologies, Moscow, Russia, 2002, 5121: 376-384.
- [7] Xie J. Dual beam laser welding[J]. Welding Journal, 2002, 81(10): 223-230.

作者简介: 雷正龙, 男, 1977 年出生, 博士, 副教授. 主要从事激光复合加工基础与应用、特种材料激光加工技术以及激光焊接质量监测与控制方面的研究工作, 发表论文 40 余篇, 授权发明专利和软件著作权 6 项. Email: leizhenglong@hit.edu.cn.

measurement parameter

Analysis of silt cavitation erosion resistance of $\text{Cr}_3\text{C}_2/\text{NiCr}$ coating prepared by high velocity oxy-fuel thermal spraying

WANG Qian , WU Yuping , LI Gaiye , GUO Wenmin (College of Mechanics and Materials , Hehai University , Nanjing 210098 , China) . pp 35 – 39

Abstract: A $\text{Cr}_3\text{C}_2/\text{NiCr}$ coating was prepared on 1Cr18Ni9Ti stainless steel by high velocity oxy-fuel (HVOF) thermal spraying. Phases and microstructures of the coating were analyzed by X-ray diffraction (XRD) , transmission electron microscope (TEM) and scanning electron microscopy (SEM) , respectively. The cavitation erosion resistance and silt erosion resistance of the coating were evaluated under two experimental conditions (fresh water and water contained fine silt) , and compared with hydro machine material 1Cr18Ni9Ti stainless steel. The result shows that the coating shows a layered structure and contains un-melted particles and some pores. The phases of the coating are composed of Cr_3C_2 , Cr_7C_3 , Cr_{23}C_6 and NiCr. The 1Cr18Ni9Ti stainless steel produces the work hardening , which results in the resistance to cavitation erosion. The $\text{Cr}_3\text{C}_2/\text{NiCr}$ coating exhibits significantly higher microhardness than 1Cr18Ni9Ti stainless steel , which leads to the resistance to silt erosion of the coating. The mass loss of the coating usually happens at the edges of the pores while the cavitation damage of the 1Cr18Ni9Ti stainless steel happens at the grain boundary and twin boundary.

Key words: high velocity oxy-fuel; silt erosion; $\text{Cr}_3\text{C}_2/\text{NiCr}$ coating; 1Cr18Ni9Ti stainless steel

Effect of process parameters on porosity formation ratio in dual-beam laser welding of aluminum alloys with filler wire

LEI Zhenglong¹ , LI Ying¹ , CHEN Yanbin¹ , SUN Zhongshao² , ZHANG Yikun² (1. State Key Laboratory of Advanced Welding and Joining , Harbin Institute of Technology , Harbin 150001 , China; 2. Capital Aerospace Machinery Company , Beijing 100076 , China) . pp 40 – 44

Abstract: The characterizations of porosity in dual-beam laser welding with filler wire of LF6 aluminum alloys were studied. Compared with the single beam laser welding with filler wire and the dual-beam laser self-fusible welding , the dual-beam laser welding with filler wire can restrain the porosity formation. Especially , the dual-beam laser welding with parallel arrangement has a better effect on inhibition of porosity. Furthermore , the effects of shielding gas component and laser energy on porosity formation ratio were analyzed. The results show that , when the helium is used as the shielding gas , the area of plasma decreases as well as the shielding effect of the plasma on laser decreases , and the welding process become more stable. At the same time , the laser power must be proper , and both too high and too low laser power make the porosity formation ratio enlarged.

Key words: dual-beam laser welding with wire filling; porosity; process parameter; aluminum alloys

Rapidly tiny resistance welding of $\text{Fe}_{78}\text{Si}_9\text{B}_{13}$ amorphous foils

LING Shiquan , WU Xiaoyu , XU Bin , LUO Feng

(Shenzhen Key Laboratory of Advanced Manufacturing Technology for Mold&Die , Shenzhen University , Shenzhen 518060 , China) . pp 45 – 48

Abstract: Rapidly tiny resistance welding of $\text{Fe}_{78}\text{Si}_9\text{B}_{13}$ amorphous foils with the thickness of 30 μm was conducted by using an inversion DC resistance welding machine. The welding parameters which affect the property of amorphous foils were discussed. The high quality joints were got without welding defects and welding parameters are as follow: 2 ms welding time , 0.2 V welding voltage and 56 N welding force. The average shear strength of the joint reaches 632 MPa. XRD test shows that the joint is amorphous structure. The cooling rate in the joint reaches 7.9×10^6 K/s , which is calculated by nucleation kinetics model , and obviously higher than the critical cooling rate of amorphous $\text{Fe}_{78}\text{Si}_9\text{B}_{13}$, and effectively prevents the crystallization of weld region. The study in this paper has high practical value in engineering.

Key words: Fe-based amorphous foil; resistance welding; joint properties; nucleation kinetics

Evaluation of stress corrosion of duplex stainless steel overlay

WANG Jing¹ , ZHANG Yiliang¹ , QIU Fei¹ , WU Daowen² (1. Department of Mechanical Engineering & Applied Electronics Technology , Beijing University of Technology , Beijing 100124 , China; 2. Luoyang Shuangrui Special Equipment Co. , Ltd , Luoyang 471039 , China) . pp 49 – 53

Abstract: In order to prevent stress corrosion in petrochemical facilities , 2205 duplex stainless steel was deposited on the surface contacted with the corrosive media in projects. In order to explore the application scope and feasibility of the solution , two welding processes (automatic welding and manual welding) , three kinds of common corrosion environment (saturated hydrogen sulfide , magnesium chloride , calcium chloride) were used to evaluate its stress corrosion comprehensively at the constant tensile load based on the microanalysis of fracture , and the mathematical model of stress-life was established based on the experimental results. The results indicate that the constant tensile load threshold is 0.45 R_{eL} for automatic welding and 0.4 R_{eL} for manual welding in saturated H_2S environment , and there is an error of 17% between them. All the samples are good after 96 hours in 0.9 R_{eL} stress test with the calcium chloride environment , which shows the excellent resistance to chloride stress corrosion. But the coating cannot be used in boiling magnesium chloride environment.

Key words: duplex stainless steel; surfacing; stress corrosion

Effect of single-component activating flux on weld morphologies in A-TIG welding of aluminum alloy

YAN Keng , GAO Lihua , YANG Gang , XIAO Hailin (Provincial Key Lab of Advanced Welding Technology , Jiangsu University of Science and Technology , Zhenjiang 212003 , China) . pp 54 – 57 , 62

Abstract: A-TIG welding experiments of 6 mm 6061 aluminum alloy were carried out to investigate the effects of activating fluxes on weld appearance and macroscopic morphologies by using five kinds of single-component activating fluxes such as